Angewandte Chemie
Eine Zeitschrift der Gesellschaft Deutscher Chemiker

Supporting Information

The First High-Pressure Chromium Oxonitridoborate CrB_4O_6N—an Unexpected Link to Nitridosilicate-Chemistry

*Birgit Fuchs, Dirk Johrendt, Lkhamsuren Bayarjargal, and Hubert Huppertz**

anie_202110582_sm_miscellaneous_information.pdf

Table of contents

Experimental Procedures

High-pressure synthesis

The title compound CrB_4O_6N was obtained through a high-pressure/high-temperature experiment in a 1000 t downstroke press with a modified Walker-type module (both Max Voggenreiter GmbH, Germany) at 7 GPa and 1623 K.

The starting materials $Cr(NO_3)_3 \cdot 9H_2O$ and B_2O_3 (Strem Chemicals, Inc., Newburyport, USA, >99.9%) were ground together in the stoichiometric ratio 1:2 in an agate mortar at ambient conditions. Subsequently, the mixture was filled into an h-BN-crucible, closed with a lid of the same material (both Henze Boron Nitride Products AG, Germany) and put into an 18/11 assembly. Eight tungsten carbide cubes were used to achieve quasi-hydrostatic pressure on the sample. For a more detailed description on the experimental setup, the reader is referred to the literature.[1]

A pressure of 7 GPa was built up in 175 minutes, before the reactant mixture was heated up to 1623 K within ten minutes. This temperature was kept constant for the following ten minutes before the heating was switched off to quench the sample to room temperature. After the 525-minute decompression process, the red microcrystalline CrB_4O_6N was mechanically separated from the surrounding crucible and the dark green side phase $CrBO_3$.

Slightly bigger crystals of CrB_4O_6N could be synthesized if the sample was not quenched to room temperature but was slowly cooled down in 30 or 80 minutes instead. These attempts also led to a larger amount of unwanted green $CrBO_3$, more with increasing cooling time, which could not be completely separated from the desired CrB_4O_6N.

Syntheses at the aforementioned conditions using the starting materials Cr_2O_3 (E. Merck AG, Darmstadt, Germany, 99%), B_2O_3 and h-BN (Strem Chemicals, Inc., Newburyport, USA, >99.9%) in the stoichiometric ratio 1:3:2 also led to the title compound CrB_4O_6N. However, in these experiments, the yield was significantly less than in the experiments using chromium nitrate as a starting material and the main product was the green $CrBO_3$.

Powder X-ray diffraction

A Stoe Stadi P powder diffractometer (STOE & Cie GmbH, Darmstadt, Germany) equipped with a Mythen 1K microstrip detector (Dectris) was used to characterize a flat sample of CrB_4O_6N which was mechanically separated from the crucible and side phase as thoroughly as possible. The measurement was performed in transmission geometry with Ge(111)-monochromatized Mo-$K_{\alpha 1}$ radiation (λ = 0.7093 Å) and a 2θ range of 2-52° was analysed with a step size of 0.015°. Additionally, a Rietveld refinement employing the TOPAS 4.2 software[2] was performed in comparison with the values derived from the single-crystal structure analysis.

Single-crystal X-ray analysis

For the single-crystal structure determination, a Bruker D8 Quest Kappa diffractometer with monochromatized Mo-K_α radiation (λ = 0.7107 Å) was employed, equipped with an Incoatec microfocus X-ray tube and a Photon 100 CMOS detector. The structure solution and parameter refinement was performed with Direct Methods using SHELXS[3] and the refinement against $|F_o|^2$ was done with SHELXL, both implemented in the WINGX software.[4] All atoms were refined with anisotropic displacement parameters and the atomic coordinates standardized with the software STRUCTURE TIDY[5] as implemented in PLATON.[6]

Second-harmonic generation measurements

Second-harmonic generation (SHG) measurements were performed on a CrB_4O_6N powder-sample. The fundamental pump wave was created with a Q-switched Nd:YAG laser (1064 nm, 5–6 ns, 2 kHz). The generated SHG signal was collected on ten different areas of the sample to check its homogeneity and averaged afterwards. A background correction of the measured intensities was carried out using signals collected between the laser pulses. α-Al_2O_3 and quartz were used as reference materials.

A detailed description of the experimental setup for the powder SHG measurement is given by Bayarjargal et al.[7]

Vibrational Spectroscopy

The FTIR-ATR (Attenuated Total Reflection) spectrum of a CrB_4O_6N powder sample with $CrBO_3$ as a side phase was measured in the spectral range of 400-4000 cm^{-1} using a Bruker ALPHA Platinum-ATR spectrometer. It is equipped with a 2×2 mm diamond ATR-crystal and a DTGS detector. 320 scans of the sample were recorded, and afterwards corrected for atmospheric effects employing the OPUS 7.2 software.[8]

DFT calculations

First-principles electronic structure calculations were performed using the Vienna ab initio simulation package (VASP 5.4.4)[9] based on density functional theory (DFT) and plane wave basis sets. Projector-augmented waves (PAW)[10] were used and contributions of correlation and exchange were treated within the generalized gradient approximation (GGA) using the PBE,[11] PBEsol,[12] and SCAN[13] functionals. The *k*-space was sampled with the Monkhorst-Pack[14] scheme using a 17 × 17 × 9 grid. Convergence criteria were 10^{-8} eV for the total energy and 10^{-4} eV/Å for the structural relaxations regarding ion positions, respectively, with a plane wave cut-off energy of 500 eV. Phonon dispersions were calculated from interatomic force constants of a 2×2×2 supercell using the PHONOPY[15] code. Electronic and phonon band dispersions were plotted with the SUMO package.[16] Infrared spectra were calculated from force constants via the dipole approach with the program IR.[17]

Results and Discussion

Crystal Structure

A close relationship of the six-membered rings in the *ab*-plane of CrB_4O_6N could be found to the rings of BO_4 tetrahedra in other borate structures, for example in CdB_2O_4,[18] *α*-FeB_2O_4,[19] and $MB_6O_9(OH)_3$ (*M* = Sc, In).[20] In these compounds, the six-membered rings can be characterized through the orientation of the BO_4 tetrahedra in the layer – downwards D or upwards U. The aforementioned borates for example show the sequences UDUDUD and UUUDDD in the cadmium-compound, UUDUDD in the iron-compound, and DDDDDD and UUUUUU in the scandium- and indium-compound. Applying this concept to the six-membered rings of BO_3N tetrahedra in the presented chromium oxonitridoborate, the sequence UUUUUU is obtained, similar to half of the six-membered rings in $MB_6O_9(OH)_3$ (*M* = Sc, In). Looking only at the anions, an alternating arrangement of three oxygen and three nitrogen atoms is observed in the six-membered rings with the nitrogen anions positioned at the corners of the rings. These layers in the *ab*-plane are interconnected via the $B2O_3N$ tetrahedra to form a network in which all tetrahedra point towards the direction $[00\bar{1}]$, leading to the formation of channels of six-membered rings alongside [100] (Figure S1). Here, there are only two nitrogen atoms involved in the direct formation of one six-membered ring, with one of the corners being occupied by oxygen.

The B–O distances in CrB_4O_6N lie in the narrow range of 1.465(2) to 1.478(3) Å. The average B–O distance of 1.471 Å fits to the average B–O bond length of 1.476(35) Å for BO_4 tetrahedra observed by Zobetz.[21] The B–N bond lengths are 1.608(3) Å within the tetrahedra in the *ab*-plane layers and 1.569(6) Å in the interconnecting tetrahedra. This is significantly longer than in the other known oxonitridoborates $Sr_3(B_3O_3N_3)$ (B–N: 1.438-1.491 Å),[22] $Eu_5(BO_{2.51}N_{0.49})_4$ (B–O/N: 1.360-1.411 Å for the mixed O/N positions)[23], and $La_3(OBN_2)O_2$ (B–N: 1.461 Å)[24]. However, these three compounds only feature threefold coordinated boron atoms in trigonal planar entities. In $Sr_3(B_3O_3N_3)$, two neighboring boron atoms in the cyclic $[B_3O_3N_3]^{6-}$ groups share one nitrogen atom, the oxygen atoms are on the outer corner of the three-membered rings. The europium oxonitridoborate consists of isolated trigonal planar units, where two of the nine crystallographically independent borate ions show a mixed oxygen/nitrogen occupancy of $BO_{1.38}N_{1.62}$ and $BO_{1.68}N_{1.32}$. Isolated BON_2 groups can be found in

$La_3(OBN_2)O_2$ in a staggered alignment. In contrast, our new chromium oxonitridoborate CrB_4O_6N features for the first time BO_3N tetrahedra, which also provide an explanation for the longer bonds, as a result of the increased coordination number of the boron atoms. A better comparison can be drawn to cubic BN, where every boron atom is tetrahedrally coordinated by nitrogen and vice versa. The B–N distance in c-BN is 1.565 Å,[25] which is around the bond lengths of 1.569 and 1.608 for the fourfold coordinated nitrogen atoms in CrB_4O_6N. This is also in good agreement with the B–N distance of 1.605 Å in the ammine borate $Cd(NH_3)_2[B_3O_5(NH_3)]_2$.[26] The O–B–O and O–B–N angles range between 107.1(2) and 112.1(2)° with an average of 109.46°, which is in accordance with the expected ideal tetrahedral angle. Table S33 and S4 display all the bond lengths and angles.

Identifying the source of the nitrogen atoms in CrB_4O_6N posed a real challenge. From our experience, nitrate as in our educt $Cr(NO_3)_3 \cdot 9H_2O$ poses a good leaving group and does not participate in the reaction, when no platinum capsule is applied. In all successful experiments that led to the red CrB_4O_6N, the crucible material h-BN was always in contact to the educt mixture, leading to the conclusion that it plays a vital part in the formation of the title compound by providing the nitrogen atoms for the reaction. Moreover, the oxonitridoborate CrB_4O_6N was found almost exclusively on the side of the product mixture (the middle being mostly green $CrBO_3$), right next to the crucible material. Additionally, the mechanical separation of CrB_4O_6N from the crucible material was challenging, giving further proof of the essential role of h-BN for the formation of CrB_4O_6N.

Table S1: Atomic coordinates and equivalent isotropic displacement parameters U_{eq} (Å^2) of CrB_4O_6N (standard deviations in parentheses).

Atom	Wyckoff position	*x*	*y*	*z*	U_{eq}
Cr1	2*b*	⅓	⅔	0.0720(5)	0.0017(2)
B1	6*c*	0.8313(3)	0.1687(3)	0.2599(5)	0.0031(3)
B2	2*a*	0	0	0	0.0025(7)
O1	6*c*	0.5113(2)	0.4887(2)	0.2095(5)	0.0029(3)
O2	6*c*	0.8456(2)	0.1544(2)	0.4361(5)	0.0038(3)
N1	2*a*	0	0	0.1879(7)	0.0023(5)

Table S2: Anisotropic displacement parameters U_{ij} (Å^2) of CrB_4O_6N (standard deviations in parentheses).

Atom	U_{11}	U_{22}	U_{33}	U_{12}	U_{13}	U_{23}
Cr1	0.0017(2)	0.0017(2)	0.0014(2)	0	0	0.00084(6)
B1	0.0035(6)	0.0035(6)	0.0024(7)	0.0000(4)	0.0000(4)	0.0019(7)
B2	0.0018(9)	0.0018(9)	0.004(2)	0	0	0.0009(5)
O1	0.0018(4)	0.0018(4)	0.0044(5)	0.0007(3)	–0.0007(3)	0.0005(4)
O2	0.0061(5)	0.0061(5)	0.0016(6)	–0.0001(3)	0.0001(3)	0.0049(5)
N1	0.0030(7)	0.0030(8)	0.0006(2)	0	0	0.0015(4)

Table S3: Interatomic B–O/B–N and Cr–O distances /Å for CrB_4O_6N (standard deviations in parentheses).

B1	–O1	1.477(2)	2×	B2	–O2	1.465(2)	3×	Cr1	–O2	1.947(2)	3×
	–O2	1.478(3)			–N1	1.569(6)			–O1	1.948(2)	3×
	–N1	1.608(3)									
$\bar{d}$		**1.51**		$\bar{d}$		**1.491**		$\bar{d}$		**1.9475**	

Table S4: Bond angles /deg for CrB_4O_6N (standard deviations in parentheses).

O2–B1–N1	107.0(2)		O2–B2–O2	107.5(2)	3×	O1–Cr1–O1	88.8(1)	3×
O1–B1–O1	107.2(2)		O2–B2–N1	111.4(2)	3×	O2–Cr1–O2	89.5(1)	3×
O2–B1–O1	109.2(2)	2×				O1–Cr1–O2	90.9(1)	6×
O1–B1–N1	112.1(2)	2×				**Ø$_{90}$**	90.03	
Ø	**109.47**		**Ø**	**109.45**		O1–Cr1–O2	179.5(1)	3×

Table S5: Comparison of the standardized atomic coordinates of CrB_4O_6N and $BaYbSi_4N_7$ (standard deviations in parentheses).

Wyckoff position	Atom	*x*	*y*	*z*	Atom	*x*	*y*	*z*
2*b*	Cr1	⅓	⅔	0.0720(5)	Yb1	⅓	⅔	0.0776(1)
2*b*					Ba1	⅓	⅔	0.4512(1)
6*c*	B1	0.8313(3)	0.1687(3)	0.2599(5)	Si1	0.8257(1)	0.1743(2)	0.2667(2)
2*a*	B2	0	0	0	Si2	0	0	0.0000(2)
6*c*	O1	0.5113(2)	0.4887(2)	0.2095(5)	N1	0.5113(5)	0.4887(3)	0.2144(3)
6*c*	O2	0.8456(2)	0.1544(2)	0.4361(5)	N2	0.8466(3)	0.1534(5)	0.4408(3)
2*a*	N1	0	0	0.1879(7)	N3	0	0	0.1922(4)

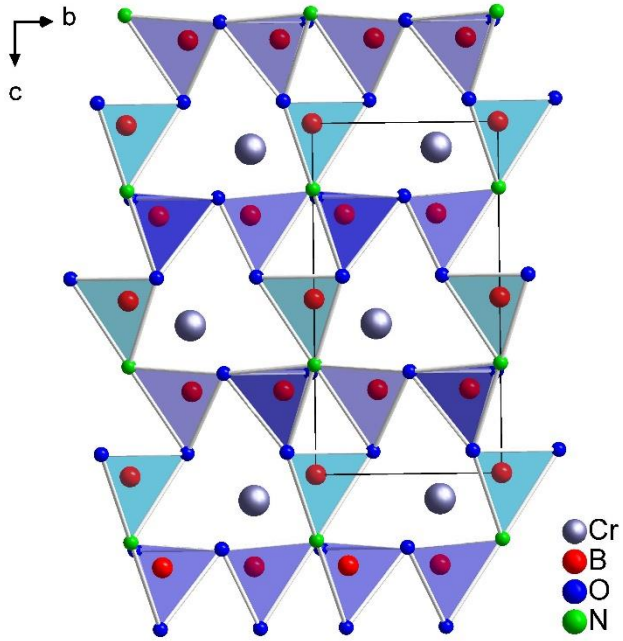

Figure S1: CrB_4O_6N is built up of three- and six-membered rings alongside the *a*-axis (tetrahedra with the central atom B1 in dark blue and with the central atom B2 in light blue).

Second-harmonic generation measurements

Table S6: SHG intensities of a CrB_4O_6N powder-sample compared to two reference materials.

Sample (Size)	SHG intensity /mV	I_{SHG}/I_{quartz} ·100%
Quartz (5-10 micrometer)	50.2 (7.8)	100.0
α-Al_2O_3 (9 micrometer)	0.2 (1.0)	0.4
CrB_4O_6N (<5 micrometer)	**41.2 (20.1)**	**82.07**

Vibrational Spectroscopy

In general, stretching vibrations of tetrahedral BO_4 groups can be found in the region of 800–1200 cm^{-1}.[27] This also seems to be the case for the BO_3N entities in CrB_4O_6N since the strongest absorption bands can be found in the same area and is also confirmed by theoretical calculations (see the red spectrum in Figure 5). In contrast to cubic boracites, that feature a fourfold coordinated oxygen atom similar to the fourfold coordinated nitrogen atom in CrB_4O_6N, the strongest band occurs at around 1000 cm^{-1}. In the boracites, the stretching vibration is shifted to higher wavenumbers due to the strong distortion of the BO_4 tetrahedra around the fourfold coordinated oxygen atom.[28] A drawing of the strongest A1-Mode in CrB_4O_6N, the B–N stretching vibration, can also be seen in the insert in Figure S2, the spectrum up to 3600 cm^{-1} is shown in Figure S3. Signals at ~1200 cm^{-1} can be assigned to the trigonal BO_3-groups of the by-product $CrBO_3$ (see the blue spectrum in Figure 5). Signals below ~800 cm^{-1} can be assigned to O–B–O bending and Cr–O vibrations.

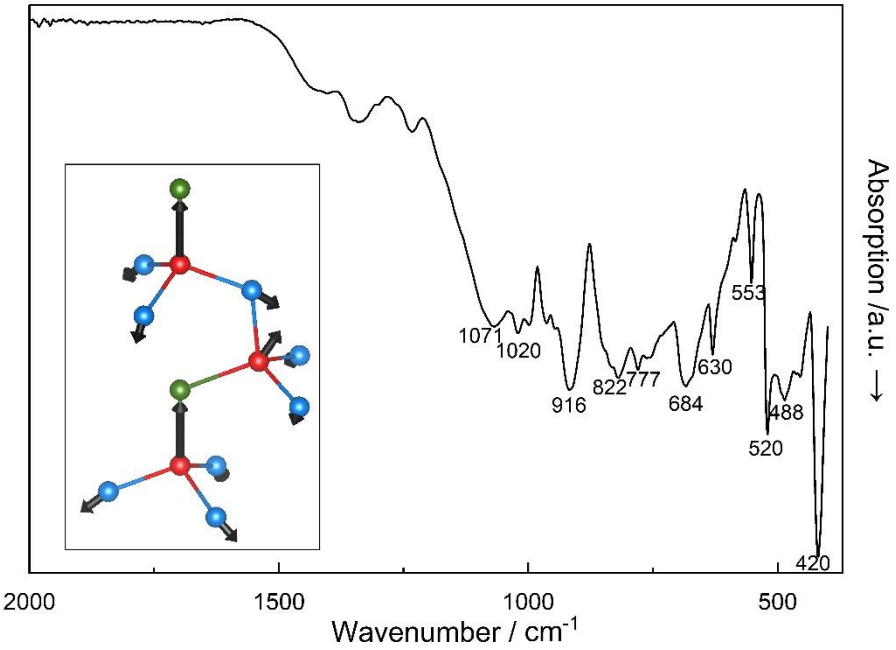

Figure S2: FTIR-ATR spectrum of a powder-sample containing CrB_4O_6N and $CrBO_3$. The insert shows a visual representation of the strongest A1-Mode (B in red, O in blue, N in green).

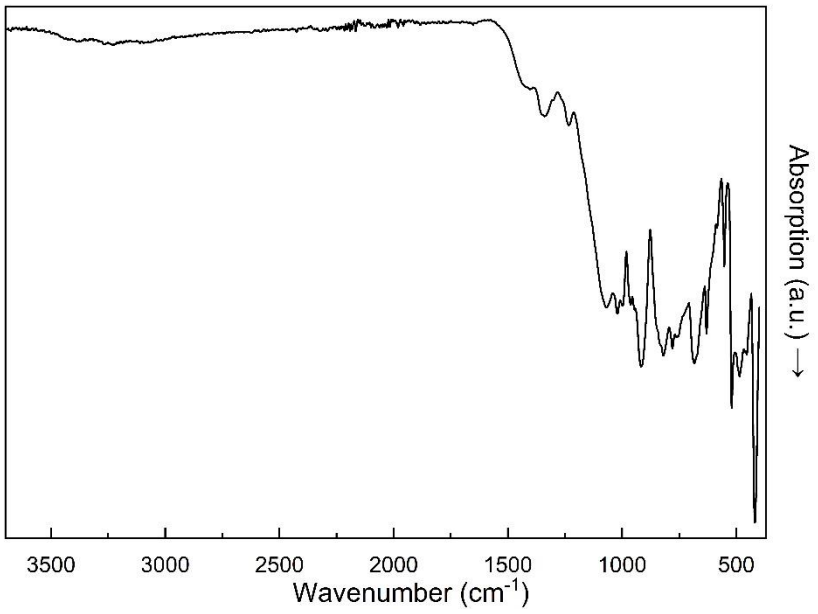

Figure S3: FTIR-ATR spectrum of a powder-sample containing CrB_4O_6N and $CrBO_3$ in the spectral range of 400–3600 cm^{-1}.

DFT calculations

Table S7: Results of the structure relaxations with different functionals.

	Experiment	PBE	PBEsol	SCAN
a, Å	5.1036(1)	5.1377 [+0.7%]	5.1003 [-0.06%]	5.0923 [-0.2%]
c, Å	8.3519(3)	8.4063 [+0.7%]	8.3471 [-0.06%]	8.3334 [-0.06%]
V, Å^3	188.40(1)	192.16 [+2.0%]	188.04 [-0.2%]	187.15 [-0.7%]
B_0, GPa	-	256.6	271.9	279.8
E_G, eV	-	1.96 i, 2.00 d	1.97 i, 2.01 d	1.65 i, 1.69 d

Table S8: Magnetism calculated with different functionals.

	PBE		PBEsol		SCAN	
	ΔE (kJ/mol)	μ(μ_B)	ΔE (kJ/mol)	μ(μ_B)	ΔE (kJ/mol)	μ(μ_B)
NM	+168.2	0	+155.7	0	+159.3	0
FM	+0.15	2.82	+0.26	2.80	+0.01	2.91
AFM	0	2.81	0	2.80	0	2.91

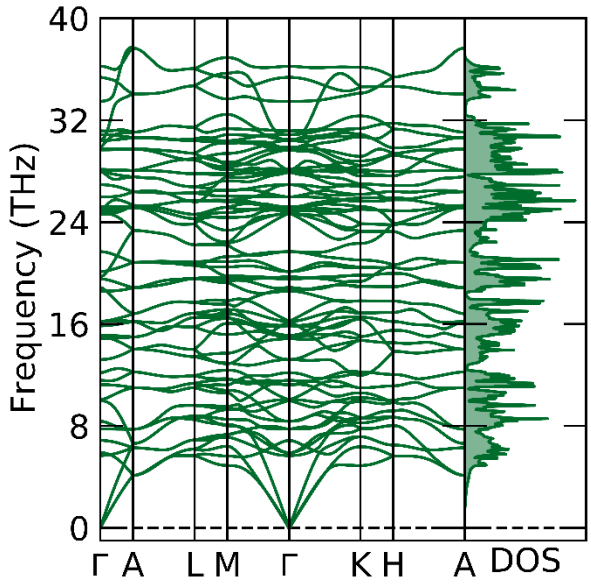

Figure S4: Phonon dispersion and phonon-DOS of CrB_4O_6N (PBEsol).

References

[1] a) D. Walker, M. A. Carpenter, C. M. Hitch, *Am. Mineral.* **1990**, *75*, 1020-1028; b) D. Walker, *Am. Mineral.* **1991**, *76*, 1092-1100; c) H. Huppertz, *Z. Kristallogr.* **2004**, *219*, 330-338.

[2] *Bruker TOPAS, v4.2,* Bruker AXS Inc., Madison, WI, USA, **2009.**

[3] a) G. M. Sheldrick, *Acta Crystallogr.* **2008**, *A64*, 112-122; b) G. M. Sheldrick, *Acta Crystallogr.* **2015**, *C71*, 3-8.

[4] L. J. Farrugia, *J. Appl. Crystallogr.* **2012**, *45*, 849-854.

[5] L. M. Gelato, E. Parthé, *J. Appl. Crystallogr.* **1987**, *20*, 139-143.

[6] A. L. Spek, *Acta Crystallogr.* **2009**, *D65*, 148-155.

[7] L. Bayarjargal, C. J. Fruhner, N. Schrodt, B. Winkler, *Phys. Earth Planet. Inter.* **2018**, *281*, 31-45.

[8] *Bruker OPUS, v7.2,* Bruker, Billerica, MA, USA, **2012.**

[9] a) G. Kresse, J. Hafner, *Phys. Rev. B* **1994**, *49*, 14251-14269; b) G. Kresse, J. Furthmüller, *Comput. Mater. Sci.* **1996**, *6*, 15-50.

[10] P. E. Blöchl, *Phys. Rev. B* **1994**, *50*, 17953-17979.

[11] J. P. Perdew, K. Burke, M. Ernzerhof, *Phys. Rev. Lett.* **1996**, *77*, 3865-3868.

[12] J. P. Perdew, A. Ruzsinszky, G. I. Csonka, O. A. Vydrov, G. E. Scuseria, L. A. Constantin, X. Zhou, K. Burke, *Phys. Rev. Lett.* **2008**, *100*, 136406.

[13] J. Sun, A. Ruzsinszky, J. P. Perdew, *Phys. Rev. Lett.* **2015**, *115*, 036402.

[14] H. J. Monkhorst, J. D. Pack, *Phys. Rev. B* **1976**, *13*, 5188-5192.

[15] A. Togo, I. Tanaka, *Scripta Materialia* **2015**, *108*, 1-5.

[16] A. M. Ganose, A. J. Jackson, D. O. Scanlon, *Journal of Open Source Software* **2018**, *3*, 717.

[17] a) J. George, R. Dronskowski, *JaGeo/IR: IR (Version 1.0.4). Zenodo*, **2019**, http://doi.org/10.5281/zenodo.3241592; b) A. L. Görne, J. George, J. Van Leusen, R. Dronskowski, *Inorganics* **2017**, *5*, 10.

[18] J. S. Knyrim, H. Emme, M. Doblinger, O. Oeckler, M. Weil, H. Huppertz, *Chem. – Eur. J.* **2008**, *14*, 6149-6154.

[19] J. S. Knyrim, H. Huppertz, *J. Solid State Chem.* **2008**, *181*, 2092-2098.

[20] a) B. Fuchs, H. Huppertz, *Z. Naturforsch.* **2020**, *75b*, 597-603; b) D. Vitzthum, L. Bayarjargal, B. Winkler, H. Huppertz, *Inorg. Chem.* **2018**, *57*, 5554-5559.

[21] E. Zobetz, *Z. Kristallogr.* **1990**, *191*, 45-57.

[22] S. Schmid, W. Schnick, *Z. Anorg. Allg. Chem.* **2002**, *628*, 1192-1195.

[23] H. A. Höppe, K. Kazmierczak, C. Grumbt, L. Schindler, I. Schellenberg, R. Pöttgen, *Eur. J. Inorg. Chem.* **2013**, *2013*, 5443-5449.

[24] T. Dierkes, M. Ströbele, H.-J. Meyer, *Z. Anorg. Allg. Chem.* **2014**, *640*, 1275-1279.

[25] R. H. Wentorf Jr., *J. Chem. Phys.* **1957**, *26*, 956-956.

[26] G. Sohr, N. Ciaghi, M. Schauperl, K. Wurst, K. R. Liedl, H. Huppertz, *Angew. Chem. Int. Ed.* **2015**, *54*, 6360-6363.

[27] R. Kaindl, G. Sohr, H. Huppertz, *Spectrochim. Acta A* **2013**, *116*, 408-417.

[28] S. C. Neumair, J. S. Knyrim, O. Oeckler, R. Kaindl, H. Huppertz, *Z. Naturforsch.* **2011**, *66b*, 107-114.